

**Structure, local ordering and mechanical properties of  
free-standing Uretane/Urea elastomer films undoped and doped  
with ferro-nanoparticles**

C. Sena

*Instituto de Física, Universidade de São Paulo,  
caixa postal 66318, 05314-970, São Paulo, São Paulo, Brazil*

M.H. Godinho

*Faculdade de Ciências e Tecnologia e CENIMAT/I3N,  
Universidade Nova de Lisboa, Quinta da Torre, P-2829-519 Caparica, Portugal.*

P.J. Sebastião

*Centro de Física da Matéria Condensada,  
Av. Prof. Gama Pinto 2, 1649-003, Lisboa,  
Portugal, and Departamento de Física,  
Instituto Superior Técnico, TU Lisbon,  
Av. Rovisco Pais 1, 1049-001 Lisboa, Portugal*

D. Sousa

*DEEC AC-Energia, Instituto Superior Técnico, TU Lisbon,  
Av. Rovisco Pais 1, 1049-001, Lisboa, Portugal*

A.M. Figueiredo Neto

*Instituto de Física, Universidade de São Paulo,  
caixa postal 66318, 05314-970, São Paulo, São Paulo, Brazil*

(Dated: August 10, 2009)

## Abstract

We report on an experimental study of the structures of non-liquid crystalline elastomers of PU/PBDO without and with ferromagnetic nanoparticles incorporated. The study is made by using the X-ray diffraction and nuclear magnetic resonance techniques. The structure proposed for the undoped cross-linked polymer network, with characteristic distance between parallel molecules of the order of 0.46 nm is almost independent on the stretching applied. The shear casting performed in order to obtain the elastomeric films introduces an anisotropy in the backbone which tends to orient the stick-like molecules parallel to the flow. In the case of nanoparticles-doped samples, a diluted and a concentrated regimes were observed. In the dilute regime the elastomeric structure is practically unchanged when compared to that from the undoped samples. In the concentrated regime, the particles act like incrustations in the elastomeric matrix, pushing and organizing the segments between cross-linked molecules in their neighborhood. In this picture, near the particles' surfaces, the organized segment's structure, that we pictured as a *quasi*-HCP structure of the parallel segment molecules, mainly orient parallel to the casting direction.

PACS numbers: 61.64.+e; 83.80.Va; 75.50.-y; 61.25.H; 61.05.C; 47.65.Cb

## I. INTRODUCTION

In 1999, Zhao and Pinho [1] proposed an elegant method to prepare elastomers for pervaporation membranes, from polypropylene oxide/polybutadiene bi-soft segment urethane/urea prepolymers. In the synthesis, two soft segments polypropylene oxide and polybutadiene establish the cross-links between urethane and urea polymers. This type of material was shown to present different degrees of phase separation, depending on the relative concentrations of both pre-polymers [2].

Interestingly, their optical and mechanical properties were found to be remarkable. Stress-induced textures were identified in the surface of films produced with polypropylene oxide isocyanate terminated triol prepolymer (PU) and polybutadiene diol (PBDO), with periodicities varying from about 3  $\mu\text{m}$  to 10  $\mu\text{m}$  [3]. Films made from PU/PBDO were shown to present stress-induced birefringence [4–6]. Godinho and co-workers [7] used the small-angle light scattering technique to investigate the bulk structure of these elastomers in the length-scale of  $\mu\text{m}$ , and described the dynamics formation of the different patterns in thin films with and without the UV light exposure of the films.

Differently from the liquid crystal elastomers (LCE) [8, 9], the structural properties in the nanometric and subnanometric length scale of non liquid crystal elastomers from PU/PBDO were not extensively investigated. Nuclear magnetic resonance experiments performed with PU/PBDO elastomers [10] revealed that the proton spin-lattice relaxation time dispersion measured is typical of a molten chain dynamics. In this molecular length scale, the results obtained with these barely isotropic elastomers (since the casting introduces a small anisotropy on them during the film preparation) were similar to those obtained from isotropic polymer networks.

Another smart material based on elastomers is the ferrogel, which is constituted by ferromagnetic nanoparticles embedded in the elastomeric matrix [11, 12]. By the action of magnetic field gradients, ferrogels show an elongation and contraction behavior [13], leading to many different applications, from soft actuators or micromanipulators in technical fields, to applications in medicine, where they might act as artificial muscles or carriers for drugs [1, 14]. Recently, Suthar and co-workers [15] reported on the characterization of ferrogels with  $\gamma\text{-Fe}_2\text{O}_3$  and  $\text{Fe}_3\text{O}_4$  nanoparticles by using transmission electron microscopy and ultra small-angle X-ray scattering. Their analysis focused on the nanoparticles agglomera-

tion characteristics in the process of elastomer synthesis. An eventual modification of the elastomeric matrix by the presence of the nanoparticles was not reported.

It is reasonable to assume that the macroscopic properties of the elastomers and ferrogels are influenced by their nanometric structure and local ordering. In the case of the elastomers we have the molecular backbone (defined here as the segments between cross-linked molecules) and, in the case of ferrogels, the molecular backbone and the nanoparticles. Structural informations should be important not only from the fundamental point of view but also for applications [16]. In this paper we report on X-ray diffraction, nuclear magnetic resonance experiments, and mechanical essays performed with PU/PBDO elastomers and ferrogels. The experiments were performed with samples unstretched and, in some cases, subjected to a mechanical uniaxial stress. The Young modulus of the different samples were measured and the results discussed in the framework of the proposed structure.

The paper is organized as follows: in the experimental section we give details about the samples preparation and the different experimental techniques employed; in the results and discussion section the different experiments are presented and discussed, supporting the structural conclusions drawn; finally the general conclusions are summarized.

## II. EXPERIMENTAL

### A. Sample preparation

The samples are rectangular  $90 - 486 \mu\text{m}$  thick free films, prepared from polypropylene oxide based isocyanate terminated triol prepolymer (PU), molecular weight of 6000, and polybutadiene diol (PBDO), molecular weight of 2800. The synthesis of these elastomeric films was done according to the procedure described in [1]. The relative weight concentration (wt%) of PU/PBDO studied is 60/40. The sample will be named PU60.

The PU and PBDO prepolymers were dissolved in toluene, under nitrogen atmosphere. For the reaction between the end groups, a drop of the catalyst dibutyltin dilauryate was added. Following a 30 min period, during which the reaction was allowed to proceed under stirring, the solutions were simultaneously cast and sheared by moving a calibrated Gardner casting Knife, at a controlled shear rate, 5 mm/s, onto a coated glass plate, at room temperature. After curing the film in an oven at  $70 - 80^\circ\text{C}$  for 3 h, it was exposed to

air and continued curing for at least 72 h in atmospheric moisture.

Ferrofluid-doped samples were obtained by first preparing a mixture of ferrofluid (EMG911, from Ferrotec Corp.) with toluene that was left to homogenize for some minutes at room temperature under stirring. We used a surfacted ferrofluid (SFF), which consists of magnetite ( $\text{Fe}_3\text{O}_4$ , simple coated) grains in a mineral oil carrier. The particles' diameter is about 10 nm. Films of PU/PBDO elastomer (486  $\mu\text{m}$  thick) were subsequently synthesized by adding to this mixture the prepolymers PU and PBDO at 60/40 relative wt%. After adding the catalyzer, the experimental route was the same used in the previous procedure. No agglomeration of grains was observed in the film. Measuring the optical absorption coefficient, due mainly to the magnetic nanoparticles incorporated into the elastomeric matrix, we obtained the actual particles' concentrations in the samples that, in the present study were  $c_{FF} = 0.013$  vol% and 0.08 vol%. These concentrations correspond to  $2.5 \times 10^{14}$  and  $1.5 \times 10^{15}$  particles per  $\text{cm}^3$ , respectively. Assuming a homogeneous distribution of particles in the sample, the typical distance between two neighboring particles is about 160 nm and 90 nm in each case. These samples will be named PU60f.

## B. X-Ray Diffraction Setup

Elastomer samples are placed in a stretch chamber, with micrometric precision control, positioned in the X-ray diffractometer (Rigaku-Denki). The collimated (0.5 mm in diameter) and monochromatic ( $\lambda_x = 0.154$  nm) X-ray beam is oriented perpendicularly to the biggest elastomer film surface (z-axis of the laboratory frame). The voltage and current used in the X-ray tube generator are 40 kV and 30 mA, respectively. The experiments were done in the Laue geometry. The diffractograms were registered in image plates and then digitalized and analyzed in a computer. The experimental resolution, obtained from the width at half-height of a Bragg peak from a single crystal, is  $\sim 0.26 \pm 0.01$  degrees. The temperature of the experiment was fixed in  $25^\circ$  C. The x-axis of the laboratory frame is defined as the stretching direction. The scattering angle  $2\theta$  is defined between the z-axis and the direction from the specimen to the position of the diffraction in the image plate. The scattering vector modulus is defined as  $s = (2 \sin \theta) / \lambda_x$ .

The stretching chamber fix about 1 mm of the elastomeric film in both ends of the micrometric device. The length  $L_0$  is defined as the unstretched length of the sample and  $L$  is

the length under stretch. The relative stretch is defined as  $R = \Delta L/L_0$ , where  $\Delta L = L - L_0$ . The stretching direction coincides with that of the casting applied during the elastomer preparation. In the present study  $R \leq 0.22$  to avoid the film rupture.

### C. The Nuclear Magnetic Resonance setup

The proton spin-lattice relaxation times  $T_1$  were obtained by using two different spectrometers, in order to cover a broad frequency range from 10 kHz to 100 MHz [17].  $T_1$  measurements at Larmor frequencies between 10 kHz and 1 MHz were performed in a home-developed fast field-cycling spectrometer [18], with a polarization and detection field of 0.21 T (corresponding to the Larmor frequency of 8.9 MHz), and switching times of 2 – 3 ms.

The  $T_1$  data between 4 and 100 MHz were obtained in a conventional pulsed NMR Bruker spectrometer with a 0 – 2.1 T electromagnet and an Avance II 300 console, using the inversion-recovery radio-frequency pulse-sequence with phase cycling  $((\pi)_x - (\pi/2)_{x,-x})$  for suppression of the dc bias.

For frequencies below 4 MHz fast field-cycling NMR techniques were used to measure the spin-lattice relaxation time [19, 20].

Both spectrometers offer the possibility to make angular-dependent measurements, since the samples can rotate perpendicularly to the Zeeman magnetic field.

The NMR samples consisted of a some rectangular samples of a few mm<sup>2</sup> stacked on the top of each other and fixed by both ends on the sample holder. The temperature was controlled within  $\pm 0.5$  °C. The magnetization (observed through the amplitude of the FID signals) showed mono-exponential time-dependence, suggesting that a uniform  $T_1$  is established in the sample. The experimental error in the spin-lattice relaxation measurements is estimated to be less than  $\pm 10$  %.

### D. Young Modulus Setup

The mechanical properties of the samples were investigated by using an extensometer from Rheometric Scientific (Minimat Firmware version 3.1), with testing machine at 25° C. Films were cut into 12 cm  $\times$  5 cm, with the longest dimension of the sample along the casting shear direction, and perpendicular to it. The film was stretched uniaxially at a rate

of 2 mm/min, along the longest sample dimension. A mechanical property of a given sample was taken to be the average of the results of six successful measurements.

### III. RESULTS AND DISCUSSION

#### A. The X-Ray essays

##### 1. Undoped samples

The X-ray diffraction patterns of the undoped elastomers present a broad band, almost isotropically disposed around the z-axis (Fig. 1). This band will be called hereafter band 1. In Figure 2a,b the transmittance is plotted as a function of  $s$ , along the  $y$  and  $x$  directions,

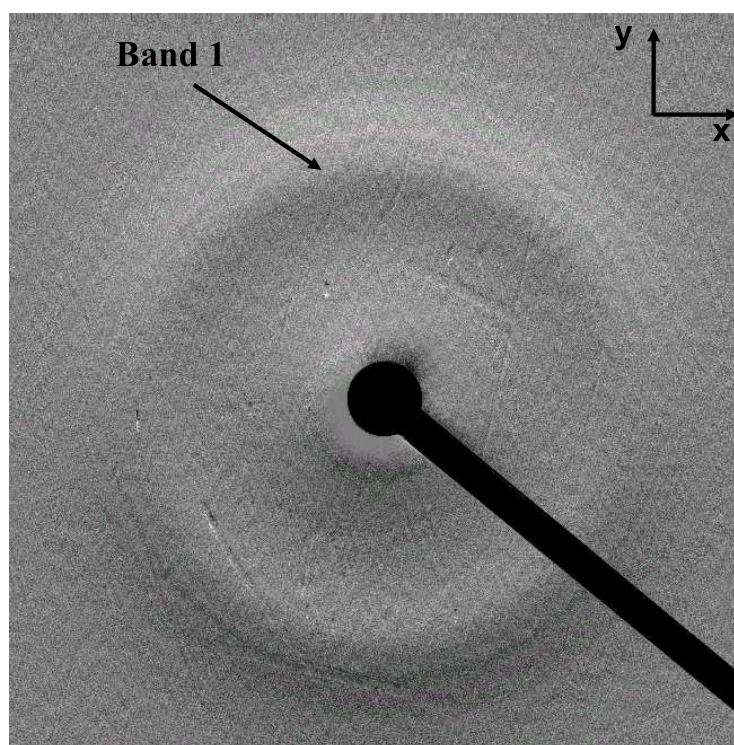


FIG. 1: Typical X-ray diffraction pattern of undoped sample PU60, unstretched. The characteristic band is identified as band 1.

respectively. The characteristic distances ( $d_{1i}$  with  $i = x, y$ ) associated to the band were found to be about  $0.45 \pm 0.02$  nm, independent on the stretching condition (Table 1). The widths at half height ( $\Delta$  - in degrees) of the band varies from  $5.67^\circ$  to  $6.00^\circ$  in both directions,

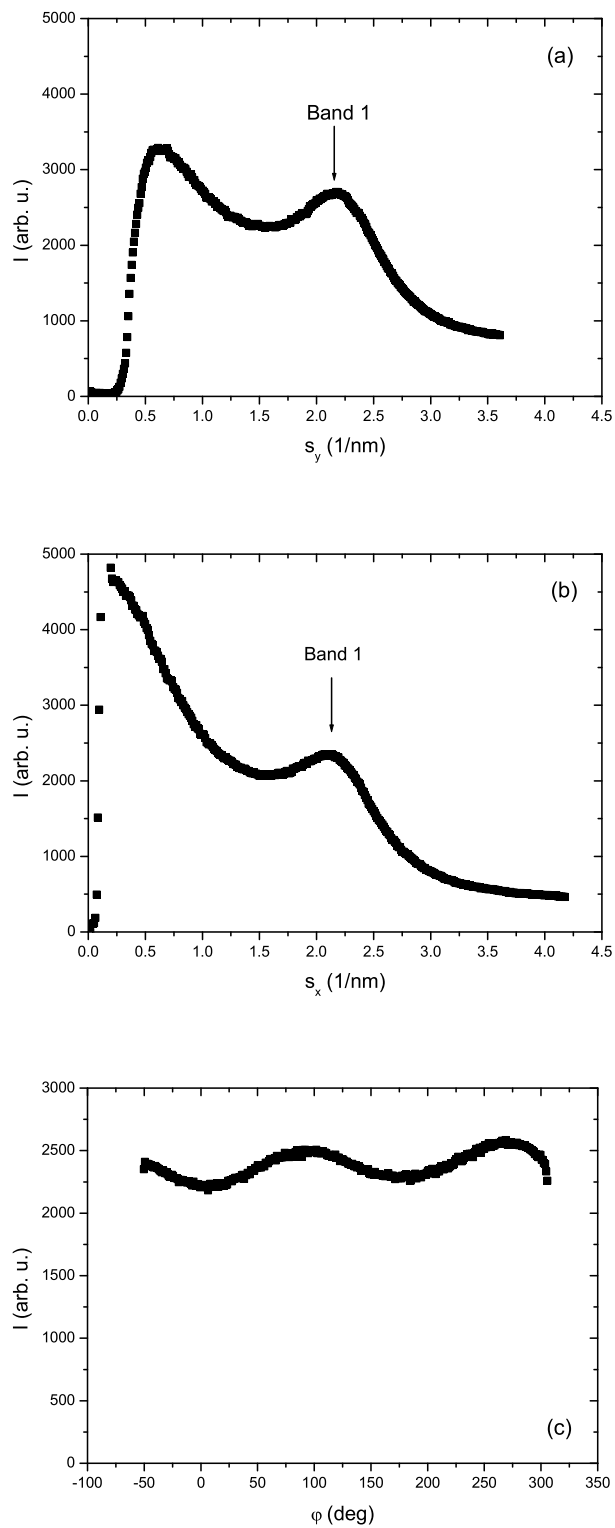


FIG. 2: Typical X-ray transmittance of undoped sample PU60, unstretched. a) as a function of  $s$ , along the y axis; b) as a function of  $s$ , along the x axis; c) as a function of the azimuthal angle  $\varphi$ .

depending on the stretching condition: the bigger  $R$  the greater (smaller)  $\Delta$  along the  $y$  ( $x$ ) direction. These values of the widths correspond, according to the Scherrer's formula [21], to correlation lengths ( $D_{1i}$ ,  $i = x, y$ ) varying from  $1.58 \pm 0.08$  nm to  $1.49 \pm 0.07$  nm, decreasing as  $R$  increases, along the  $y$  axis; and varying from  $1.42 \pm 0.07$  nm to  $1.50 \pm 0.07$  nm, increasing as  $R$  increases, along the  $x$  direction. The azimuthal angle analysis of the transmittance (angle  $\varphi$ , measured in the  $xy$  plane, starting from the  $x$ -axis, in the counterclockwise direction) revealed that the band transmittance is more intense along the  $y$ -axis (Fig. 2c).

TABLE I: Spacing distance ( $d$ ), correlation length ( $D$ ) and orientational order parameter ( $OP$ ) of the diffraction bands of the undoped and ferrofluid-doped elastomers as a function of the stretching parameter  $R$ . The subscripts ( $_1$ ,  $_2$  and  $_3$ ) refer to the parameters of the bands 1, 2 and 3.

$R \downarrow [c_{FF} = 0]$	$d_{1y}$ (nm)	$D_{1y}$ (nm)	$d_{1x}$ (nm)	$D_{1x}$ (nm)	$OP_1$
0	$0.45 \pm 0.02$	$1.58 \pm 0.08$	$0.47 \pm 0.02$	$1.42 \pm 0.07$	$0.60 \pm 0.02$
0.08	$0.45 \pm 0.02$	$1.55 \pm 0.08$	$0.47 \pm 0.02$	$1.44 \pm 0.07$	$0.56 \pm 0.02$
0.15	$0.45 \pm 0.02$	$1.52 \pm 0.08$	$0.47 \pm 0.02$	$1.46 \pm 0.07$	$0.58 \pm 0.02$
0.21	$0.45 \pm 0.02$	$1.49 \pm 0.07$	$0.46 \pm 0.02$	$1.50 \pm 0.07$	$0.61 \pm 0.02$
$R \downarrow [c_{FF} = 0.013 \text{ vol}\%]$					
0	$0.46 \pm 0.02$	$1.50 \pm 0.08$	$0.46 \pm 0.02$	$1.46 \pm 0.07$	$0.60 \pm 0.02$
0.08	$0.46 \pm 0.02$	$1.53 \pm 0.08$	$0.47 \pm 0.02$	$1.50 \pm 0.07$	$0.57 \pm 0.02$
0.15	$0.46 \pm 0.02$	$1.50 \pm 0.07$	$0.46 \pm 0.02$	$1.51 \pm 0.07$	$0.55 \pm 0.02$
0.21	$0.44 \pm 0.02$	$1.50 \pm 0.07$	$0.47 \pm 0.02$	$1.50 \pm 0.07$	$0.60 \pm 0.02$
$R \downarrow [c_{FF} = 0.08 \text{ vol}\%]$					
0	$0.47 \pm 0.02$	$1.54 \pm 0.08$	$0.47 \pm 0.02$	$1.50 \pm 0.07$	$0.60 \pm 0.02$
0.22	$0.46 \pm 0.02$	$1.53 \pm 0.08$	$0.47 \pm 0.02$	$1.48 \pm 0.07$	$0.60 \pm 0.02$
$R \downarrow [c_{FF} = 0.08 \text{ vol}\%]$	$d_{2y}$ (nm) $\downarrow$	$D_{2y}$ (nm) $\downarrow$	$d_{2x}$ (nm) $\downarrow$	$D_{2x}$ (nm) $\downarrow$	$OP_2$ $\downarrow$
0	$0.30 \pm 0.12$	$7.80 \pm 0.39$	$0.30 \pm 0.12$	$9.67 \pm 0.48$	$0.63 \pm 0.01$
0.22	$0.30 \pm 0.12$	$12.26 \pm 0.61$	$0.30 \pm 0.12$	$9.79 \pm 0.49$	$0.64 \pm 0.01$
$R \downarrow [c_{FF} = 0.08 \text{ vol}\%]$	$d_{3y}$ (nm) $\downarrow$	$D_{3y}$ (nm) $\downarrow$	$d_{3x}$ (nm) $\downarrow$	$D_{3x}$ (nm) $\downarrow$	$OP_3$ $\downarrow$
0	$0.26 \pm 0.01$	$10.25 \pm 0.51$	$0.26 \pm 0.01$	$10.25 \pm 0.51$	$0.62 \pm 0.02$
0.22	$0.25 \pm 0.01$	$9.81 \pm 0.49$	$0.25 \pm 0.01$	$11.03 \pm 0.55$	$0.60 \pm 0.02$

## 2. Ferrofluid-doped samples

In the case of the sample doped with  $c_{FF} = 0.013$  vol% the diffraction pattern has the same characteristics of those of Fig. 1, with only one broad band (band 1). The values of  $d_1$  ( $\sim 0.45$  nm) and  $D_1$  ( $\sim 1.52$  nm) remain comparable to those from the undoped samples (Table 1). Still here,  $D_{1x}$  presented a tendency to increase with  $R$ .  $D_{1y}$  however, remained

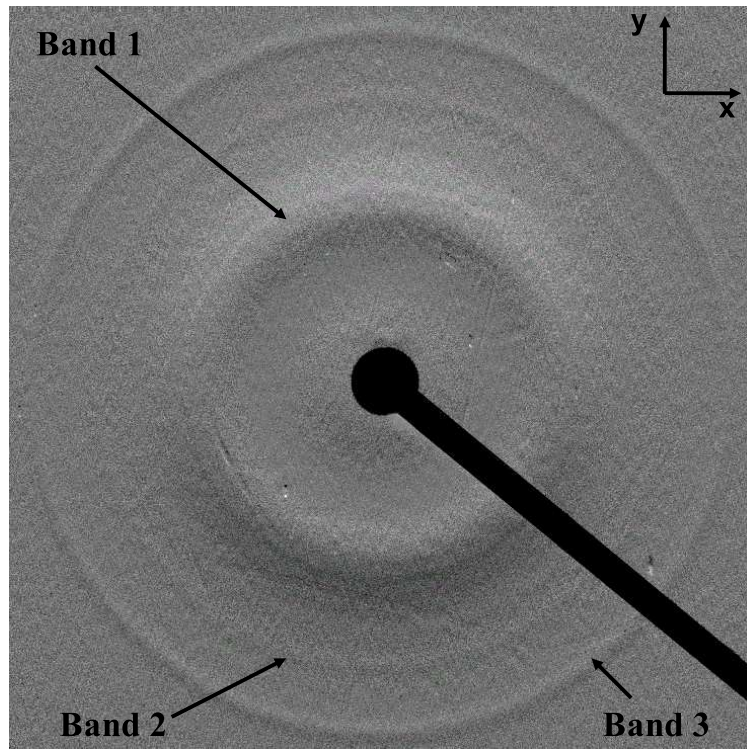


FIG. 3: Typical X-ray diffraction pattern of ferrofluid doped sample with  $c_{FF} = 0.08\text{vol}\%$ , unstretched. The characteristic bands are identified as band 1, 2 and 3.

almost independent on  $R$ . The band transmittance is also more intense along the y-axis direction.

With  $c_{FF} = 0.08$  vol%, besides the band 1, two others almost isotropic finer bands are visible at larger angles (Fig. 3). These bands will be called hereafter band 2 and band 3. Band 3 is more intense than band 2. This last one appears like a shoulder in Fig. 4a where the typical transmittance as a function of  $s$  is plotted. The characteristic distances of these fine bands (2 and 3, respectively) are about  $0.30 \pm 0.12$  nm and  $0.26 \pm 0.01$  nm, independent on the stretching condition. The correlation lengths were shown to be

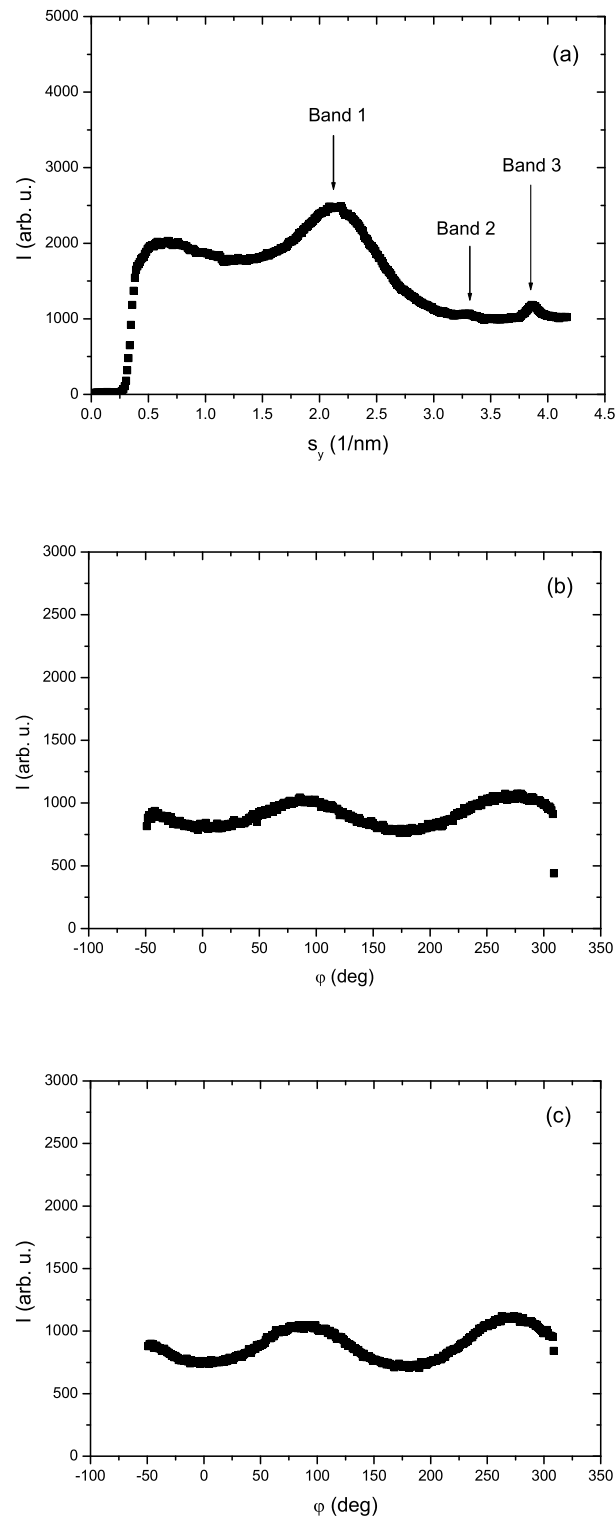


FIG. 4: Typical X-ray transmittance of ferrofluid doped sample with  $c_{FF} = 0.08\text{vol}\%$ , unstretched. a) as a function of  $s$ , along the  $y$  axis; b) as a function of the azimuthal angle  $\varphi$ , band 2; c) as a function of the azimuthal angle  $\varphi$ , band 3.

independent of the stretching condition, being about 10.0 nm for both bands. The band 1 characteristic distances are  $d_1 = 0.47 \pm 0.02$  nm and  $D_1 = 1.50 \pm 0.08$  nm. Figures 4 b and c present the transmittances and as a function of  $\varphi$  of a typical diffraction pattern of band 2 and band 3, respectively. All the three bands transmittances are more intense along the y-axis direction.

## B. The NMR essays

Figure 5 shows the  $^1\text{H}$  spin-lattice relaxation time ( $T_1$ ) as a function of the Larmour frequency ( $\nu_L$ ) of the PU60 undoped and PU60f doped with ferrofluid ( $c_{FF} = 0.013$  vol%). The temperature of the sample was set at 85 °C to improve the signal-to-noise ratio in the spectrometer. At room temperature the values of  $T_1$  at low frequencies are close the detection limit of our equipment. We experimentally verified for the undoped sample (data not shown) that the shapes of the dispersion curves ( $T_1$  versus  $\nu_L$ ) are identical, only shifted towards higher values of  $T_1$  for increasing temperatures.

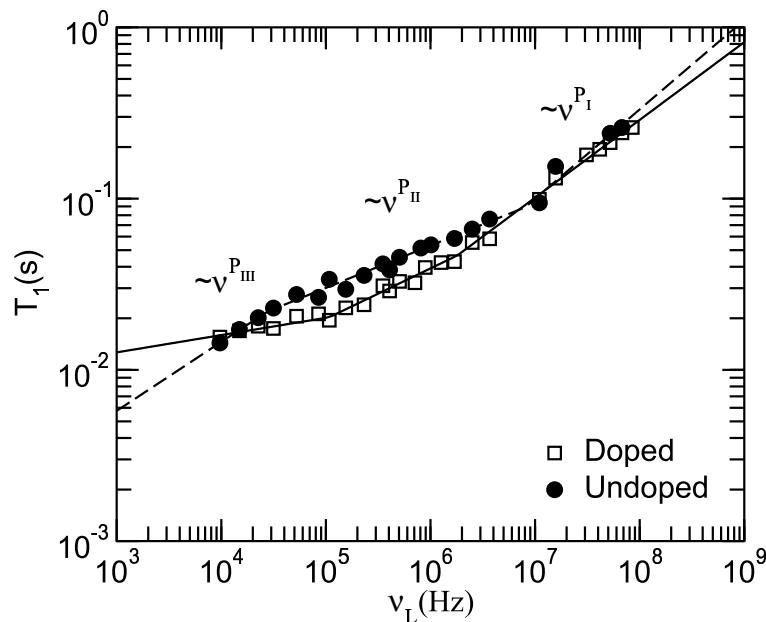


FIG. 5: Spin-lattice relaxation time ( $T_1$ ) as a function of the Larmour frequency ( $\nu_L$ ) of the undoped PU60 sample ( $\bullet$ ) and ferrofluid-doped PU60f sample with  $c_{FF} = 0.013$  vol% ( $\square$ ). The solid and dashed lines are best-fits of the renormalized Rouse model performed.

A spin-lattice relaxation time decrease with frequency is observed in all frequency region

for the two undoped and doped ( $c_{FF} = 0.013$  vol%) systems, both at 85°C and at room temperatures.

In the case of undoped samples, three linear regions can be identified and may be described in the framework of the renormalized Rouse model for the molecular dynamics of the elastomer constituents [22]. In this model  $T_1 \propto \nu_L^{P_j}$ , with  $j$  referring to the particular Larmour frequency range. The processes occurring in the first and second regions of the dispersion curves depicted in Fig. 5 ( $\nu_L \gtrsim 10^7$  Hz - region I;  $2.5 \times 10^4$  Hz  $\lesssim \nu_L \lesssim 10^7$  Hz - region II) refer to dipolar intra-segment interactions. In the third region of the dispersion curve ( $\nu_L \lesssim 2.5 \times 10^4$  Hz - region III) the processes refer to dipolar inter-segments interactions. The fitting parameters obtained with the Rouse power law in the different regions are given in Table 2. The values of the exponents for the undoped PU60 system are quite similar to others reported in the literature for other polymers [20].

TABLE II: Fitting parameters ( $P_j$  with  $j = I, II, III$ ) of the power-law dependence of  $T_1$  as a function of the Larmour frequency ( $T_1 \propto \nu_L^{P_j}$ ) and cut-off frequencies ( $f$ ) of the undoped and ferrofluid doped (with  $c_{FF} = 0.013$  vol%) elastomers.

	$P_I$	$P_{II}$	$P_{III}$	$f_{I-II}$ ( $10^5$ Hz)	$f_{II-III}$ ( $10^4$ Hz)
$c_{FF} = 0$	$0.52 \pm 0.01$	$0.25 \pm 0.01$	$0.40 \pm 0.17$	$85 \pm 1$	$2.8 \pm 0.01$
$c_{FF} = 0.013$ vol%	$0.45 \pm 0.02$	$0.30 \pm 0.03$	$0.10 \pm 0.03$	$18 \pm 9$	$11 \pm 1$

The ferrofluid-doped sample ( $c_{FF} = 0.013$  vol%) presented systematically values of  $T_1$  smaller than those obtained in undoped samples in the frequency range of  $2 \times 10^4$  Hz to about  $10^7$  Hz. The same experiment performed with magnetic grains oriented in the elastomeric matrix (by applying a magnetic field during the sample synthesis) gave the same results of unoriented particles. In the case of the doped PU60f film the values of the fitted exponents  $P_I$  and  $P_{II}$  are still within the range usually associated with the intra-segment relaxation contributions, although they are slightly smaller than those obtained for the undoped film. In the low-frequency domain the exponent  $P_{III}$  is quite different from the value obtained in the undoped film. According to the renormalized Rouse relaxation model for polymers, the relaxation observed at low-frequencies is usually associated to inter-segment relaxation contributions. Therefore, the presence of the nanoparticles in the elastomer seems

to strongly influence the relaxation contribution associated with these interactions. These results indicate that the particles affects the local ordering of the backbone molecules in the neighborhood of them. As the values of  $P_I$  and  $P_{II}$  are quite similar in the undoped and doped ( $c_{FF} = 0.013$  vol%) systems we can conclude that the intra-segment relaxation contributions are less affected by these changes in the local ordering.

At higher magnetic nanoparticles concentrations the dispersion curve could not be obtained in our experimental setups. For  $c_{FF} = 0.08$  vol% PU60f system the larger concentration of magnetic nanoparticles dispersed in the elastomer film strongly reduces the homogeneity of the magnetic field in the measuring volume, thus shortening the detected FID signal. Some values of  $T_1$  from the  $c_{FF} = 0.08$  vol% PU60f system were measured at high frequencies (between 31 MHz and 85 MHz), at the temperatures of 25°C and 85°C. The values of  $T_1$  obtained in both temperatures were similar (within our experimental uncertainty) to those obtained for the doped  $c_{FF} = 0.013$  vol% system. However, measurements at lower frequencies were not possible due to lack of radio-frequency power in our fast field-cycling NMR spectrometer.

### C. The Young Modulus essays

Table 3 shows the values of the Young modulus ( $E$ ) of the samples in different experimental situations. Let us first analyze the undoped sample (the first two columns of Table 3). The value of  $E$  when the stretching direction is parallel to the casting direction ( $E_{\parallel}$ ) is about 3 % bigger than the value when stretching direction is perpendicular to the casting direction ( $E_{\perp}$ ), in accordance with data obtained before for this kind of elastomers [23].

When the magnetic particles are incorporated in the elastomeric matrix (particles not oriented by any external magnetic field ( $c_{FF} = 0.013$  vol% and 0.08 vol%)), both moduli ( $E_{\parallel}$ ,  $E_{\perp}$ ) decrease with respect to those from undoped samples. In this case  $E_{\parallel}$  is about 9.5 % bigger than  $E_{\perp}$ . Comparing the Young moduli  $E_{\parallel}$  and  $E_{\perp}$  in the situations where the magnetic particles are oriented by an external magnetic field when incorporated in the elastomeric matrices we note that: i) the presence of magnetic nanoparticles with their magnetic moments ( $\mu$ ) parallel to the casting and stretching direction increases (by about 6 %) the value of  $E_{\parallel}$  with respect to that obtained when the particles were oriented with their magnetic moment perpendicular to the casting and stretching direction ( $\mu$  perpendicular to

TABLE III: Young modulus  $E$  of the different essays performed.  $c_{FF}$  is the concentration of magnetic particles incorporated in the elastomer in volume %. The geometry of the different essays is also presented:  $C$  and  $H$  represent the directions of the casting and the magnetic field, respectively.

$E$ ( $10^{-3}$ MPa) $\rightarrow$	$E_{//}$	$E_{\perp}$	$E_{//}^{H//C}$	$E_{\perp}^{H//C}$	$E_{//}^{H\perp C}$	$E_{\perp}^{H\perp C}$
$c_{FF} = 0$	$1809 \pm 19$	$1764 \pm 9$	—	—	—	—
$c_{FF} = 0.013$ vol%	$1733 \pm 14$	$1583 \pm 9$	$1759 \pm 9$	$1688 \pm 12$	$1656 \pm 8$	$1585 \pm 7$
$c_{FF} = 0.08$ vol%	$1527 \pm 80$	$1527 \pm 102$	$1226 \pm 102$	$1504 \pm 365$		

the biggest surface of the film); ii) the presence of magnetic nanoparticles with their magnetic moments ( $\mu$ ) perpendicular to the casting and stretching direction ( $\mu$  perpendicular to the biggest surface of the film) decreases (by about 6 %) the value of  $E_{\perp}$  with respect to that obtained when the particles were oriented with their magnetic moment parallel to the casting and perpendicular to the stretching direction ( $\mu$  parallel to the biggest surface of the film). In general, the Young moduli of samples without the magnetic nanoparticles are bigger than those obtained from ferrofluid doped samples.

#### D. Discussion about the structure

##### 1. Undoped samples

The X-ray diffraction patterns of the undoped samples are consistent with the picture of an almost isotropic elastomeric matrix formed by the backbone of PU and PBDO molecules. The casting introduces an anisotropy in the elastomeric matrix in a way that the backbone molecules are mainly oriented parallel to the casting direction. These backbones originate the band 1. This band informs about the mean distance between the backbone molecules ( $\sim 0.46$  nm). This characteristic distance (order of magnitude) seems to be typical from elastomer backbones, being encountered also in LCE [9]. The correlation length obtained reveals that the typical ordering in the elastomeric matrix extends laterally to about 3 molecules ( $D \sim 1.50$  nm). To evaluate the orientational ordering of the molecules with respect to the casting direction we measured the width at half height ( $\Delta_{1\varphi}$ , in radians)

of the X-ray transmittance peak as a function of the azimuthal angle  $\varphi$ , and evaluate an "orientational order parameter" as  $OP_1 = (\pi - \Delta_{1\varphi})/\pi$  (last column in Table 1). We observe that  $OP_1 \sim 0.60$ , practically independent on the stretching condition. This result contrasts with that from LCE where, increasing the stress, the orientational and positional ordering increase. The presence of three straight-line domains in the NMR dispersion curve (Fig. 5) characterizes the inter and intra-molecular coupling present in the backbone structure, described by the renormalized Rouse model. The structural results show that the short-range positional ordering at nanoscales along both directions, parallel and perpendicular to the casting, are almost similar. The values of the Young modulus measured inform us about the elasticity of the sample under stress in both relative directions (with respect to the cast direction). The higher values (about 3 %) of  $E$  in the direction parallel to the casting with respect to that perpendicular to it seems to be related to the anisotropy of the backbone structure at the nanometric scale. The casting introduces an anisotropic orientation of these backbones with respect to the casting direction, detected in the optical birefringence [5] and Young moduli experiments at  $R = 0$  ([23] and Table 3). The picture of the structure of the elastomeric matrix under stretch, at this length scale, is particularly interesting. It is known that some macroscopic properties (e.g., the birefringence) of this material change a lot when the elastomer is stretched [4]. Under stretch, the characteristic distance associated to the band 1 is independent on the stretch. On the other hand, the correlation distances associated to this band change as the sample is stretched: along the stretching (casting) direction  $D_{1x}$  increases with  $R$  and, perpendicularly to the stretching direction,  $D_{1y}$  decreases with  $R$ . These results reveal that the stretch progressively reduces the backbone positional ordering along the direction perpendicular to the casting/stretching direction and increases this ordering along the casting/stretching direction.

## 2. Ferrofluid-doped samples

In the case of doped samples, two regimes were observed: a diluted (e.g.,  $c_{FF} = 0.013$  vol%) and a concentrated (e.g.,  $c_{FF} = 0.08$  vol%) regime. This aspect will be discussed in more details at the end of this section.

In the dilute regime, we did not observe any significant modification in the diffraction patterns with respect to those from undoped samples. This fact indicates that the elas-

tomeric structure is unchanged (or slightly modified but undetected by our experimental diffraction method) by the presence of the magnetic nanoparticles. However, NMR experiments revealed an interesting effect in the relaxation properties of the nanoparticles-doped elastomer in this diluted regime: The third region (named *III*) of the dispersion curve shown in Fig. 5 shows a much smaller value of  $P_{III}$  when compared to that obtained in the undoped system. This fact indicates that the presence of nanoparticles in the structure weakens the dependence of  $T_1$  with the Larmour frequency in the inter-segment region of the dispersion curve. On the other hand the values of  $P_I$  and  $P_{II}$  are similar in both undoped and doped ( $c_{FF} = 0.013$  vol%) systems. Therefore, we can conclude that the intra-segment relaxation contributions are less affected by the changes in the local ordering.

It is interesting to note that NMR results reveal a modification in the local ordering of the backbone due to the nanoparticles' presence in the diluted regime when compared with the undoped sample, not yet evidenced by the X-ray diffraction experiment. This fact might be related to the different correlation lengths probed by the different techniques.

In the concentrated regime, the diffraction pattern changed, comparing with that from the sample in the diluted regime: Two others finer bands appeared at higher values of  $s$ . These bands are narrower than the band 1, indicating larger correlation lengths characteristics of the ordering. However, band 3 is more intense than band 2 (Fig. 4a). A possible origin of this ordering could be a surface-stabilizing effect where the particles' surfaces act to organize around them the elastomeric backbones. Let us assume that this ordering of the backbone molecules in the neighborhoods of the surfaces of the particles is of the *quasi*-hexagonal closed-packing type (*q*-HCP). The lattice parameter ( $a$ ) calculated with the  $d_{hkl} = d_{100} = d_{3y} \sim 0.26$  nm (see Table 1) is of the order  $a \sim 0.30$  nm ( $hkl$  are the Miller indices). The correlation length associated to this band reveals that the typical ordering in the elastomeric matrix extends to about 35 backbone molecules ( $D_3 \sim 11.0$  nm). A sketch of the structure in the concentrated regime could be pictured in the following way. As the nanoparticles are coated with a monolayer of amphiphilic molecules, the hydrophobic part of these molecules are exposed to the contact with the backbone molecules of the elastomeric matrix. The particles act like incrustations in the elastomeric matrix, pushing and organizing the backbone molecules in their neighborhood. In this picture, near the particles' surfaces, the backbones form an organized structure, that we pictured as a *q*-HCP structure of the parallel backbone molecules. Likewise band 1, band 3 presents the same type

of intensity profile as a function of the azimuthal angle  $\varphi$ , indicating that the orientational profile characteristics of the "bulk" backbone is present in the "surface" backbone: The molecules which form the backbone are mainly oriented parallel to the casting direction. We measured the orientational order parameter of this outer band  $OP_3 \sim 0.61$ , practically independent on the stretching condition. The less intense band 2 could be a residual finger print of the  $q$ -HCP structure of lattice parameter  $a \sim 0.30 \text{ nm} \sim d_2$ . This weak band should be originated by a mean characteristic distance between molecules of the backbone, closer to the ferroparticles. In a real long-range positional HCP ordering this band should disappear, however, the molecular ordering around the ferroparticles is spatially limited (see, e.g., the magnitudes of  $D_3$  and  $D_2$ ).

As discussed before, it was not possible to perform the full-frequency range measurements of  $T_1$  at the concentrated regime. However, we measured  $T_1$  in the high-frequency range (20–90 MHz) in the sample with  $c_{FF} = 0.08 \text{ vol\%}$ , and the values obtained were identical (within our experimental accuracy) to those from the samples in the diluted regime. This indicates that the intra-segment relaxation contributions are similar in both diluted and concentrated regimes. Since the X-ray patterns from the samples in the dilute and concentrated regimes are very different, we expect more important changes in the relaxation in the low-frequency range. The difference observed in the  $P_{III}$  exponent in the undoped and doped (diluted regime) samples may indicate a pre-transitional (structural) effect towards the concentrated regime. Similar results were observed in liquid crystalline systems at the isotropic-to-nematic phase transition [24].

The measurements of the Young modulus of ferrofluid doped elastomers indicate that  $E$  decreases as the ferrofluid unoriented particles are introduced in the elastomeric matrix. The differences of  $E$  obtained in the diluted and concentrated regimes, defined above, are not significant. In all the cases, the Young modulus measured in the geometry parallel ( $//$ ) to the casting direction is larger than that measured in the perpendicular ( $\perp$ ) condition. The relative decrease of  $E_{//}$  and  $E_{\perp}$ , measured in samples with the magnetic particles with respect to those obtained in undoped samples, is of the order of 4 % and 12 %, respectively. The orientation of the magnetic moments of the particles during the elastomer preparation did not provoke a significant modification in the values of  $E$  with respect to those obtained with unoriented moments. The presence of the ferrofluid particles (oriented or not) in the elastomeric matrix seems to soften the structure, in particular, in the direction

perpendicular to the casting direction. The ferrofluid particles, and the "surface" backbone organized around them, may act like defects in the previously homogeneous elastomeric structure. These defects could be the responsible for the decreasing of  $E$  in samples doped with ferroparticles.

Let us push a little more further the discussion about the existence of the two nanoparticles-doping regimes in our ferrogels, at least, in terms of the structures observed. It is not reasonable to consider that we did not observe the bands 2 and 3 in samples doped with  $c_{FF} = 0.013$  vol% only because there were not enough particles illuminated by the X-ray beam to reveal the  $q$ -HCP structure around them. As the beam collimator used had a diameter of 0.5 mm, the number of particles illuminated in the concentrated regime is only about three times larger than that from the diluted regime. This difference could not explain the complete absence of bands 2 and 3 in the diffractogram of the sample with  $c_{FF} = 0.013$  vol%. In a seminal work, Brochard and de Gennes [25] discussed, from the theoretical point of view, the physics of magnetic suspensions in liquid crystals. One of their many interesting results presented in this paper was the existence of a minimal concentration ( $c_m$ ) of anisometric particles (assumed as long cylinders of typical length  $L$ ) in a nematic matrix, above which, the average orientation of the nematic follows that of the particles. Above this minimal concentration there is a collective behavior of the nematic, following the orientation of the anisometric particles. This prediction was verified in lyotropic nematics doped with nanoparticles ( $\text{Fe}_3\text{O}_4$  double coated) from water-based ferrofluids [26]. Brochard and de Gennes predicted that  $c_m \sim 1/(LD^2)$ , where  $D$  is a typical linear dimension of a domain where the orientation of the axes of the cylindrical particles does not coincide with the fixed director orientation outside this domain. Since the effect of the host particle in the nematic matrix is screened out with at distances larger than  $\kappa^{-1}$  (where  $\kappa^2 \sim cL$ ), the nematic matrix follows the particles' orientation if  $D \gg \kappa^{-1}$ . In the other limiting case  $D \ll \kappa^{-1}$  the nematic is weakly perturbed by the particles' presence. In our ferrogels, the presence of the particles in the elastomeric matrix perturbs the structure in their vicinity, pushing the backbone molecules away from the volume occupied by the particles. The bulk structure of the elastomer may absorb this perturbation, accommodating the backbone molecules but, beyond a certain concentration, this accommodation could not be absorbed by the bulk, and a new equilibrium structure is achieved. In this framework, and using a similar approach proposed by Brochard and de Gennes, we can evaluate a typical linear dimension in the

nanoparticle-doped elastomer  $D_f \sim \sqrt{1/(c_{FF} \times L_{FF})}$ , where  $c_{FF} \sim 1.5 \times 10^{15} \text{ cm}^{-3}$  and  $L_{FF} = 10^{-6} \text{ cm}$ :  $D_f \sim 260 \text{ nm}$ . Considering that in the concentrated regime the typical distance between two neighboring particles is about 90 nm we expect to find about three particles along a linear path of length  $D_f$ . The distortion amplitude around the particles ( $\sim \kappa^{-1}$ ) may be sketched as a spherical shell of thickness of about 10 nm ( $D_3$  from the band 3), and  $D_f/D_3 \sim D_f/\kappa^{-1} \sim 26$ , which is consistent with what we would expect.

#### IV. CONCLUSIONS

The structures of non-liquid crystalline elastomers of PU/PBDO without and with ferromagnetic nanoparticles incorporated were studied by using the X-ray diffraction and nuclear magnetic resonance techniques. The structure proposed for the pure elastomer is made of a molecular backbone (i.e., a cross-linked polymer network) where the characteristic distance between cross-linked parallel segment molecules is of the order of 0.46 nm. The correlation length ( $D$ ) obtained is of the order of 1.5 nm. The casting performed in the experimental procedure to obtain the elastomeric films introduces an anisotropy in the backbone, tending to orient the stick-like molecules parallel to the casting direction. Under stretch ( $R \leq 0.22$ ), the characteristic distance between molecules is independent on the stretch. On the other hand, the correlation lengths change as the sample is stretched in a way that the stretch progressively reduces the backbone positional ordering along the direction perpendicular to the casting/stretching direction and increases this ordering along the casting/stretching direction.

In the case of nanoparticles-doped samples, two regimes were observed: A diluted (e.g.,  $c_{FF} = 0.013 \text{ vol}\%$ ) and a concentrated (e.g.,  $c_{FF} = 0.08 \text{ vol}\%$ ) regime. In the dilute regime the elastomeric structure is practically unchanged, however, NMR experiments evidence modifications in the backbone local ordering, which might be interpreted as a pre-transitional effect towards the concentrated regime. In the concentrated regime, the particles act like incrustations in the elastomeric matrix, pushing and organizing the backbone molecules in their neighborhood. In this picture, near the particles' surfaces, the backbones form an organized structure, that we pictured as a *quasi*-HCP structure of the parallel backbone molecules, mainly oriented parallel to the casting direction.

### **Acknowledgments**

The authors thank CNPq, FAPESP, CAPES/GRICES - 175/07, and INCT-FCx (Instituto Nacional de Ciência e Tecnologia de Fluidos Complexos) for financial support. This work was partially supported by POCI/CTM/56382/2004-FEDER and by Portuguese Science Foundation (FCT) through Pluriannual Contracts with CENIMAT/I3N. We thank Mr. Cristiano Paes for the image processing of Figs. 1 and 3. P. J. Sebastião and D. Sousa thank J. Cascais for the technical help in the development of the new FFC NMR spectrometer.

- 
- [1] C.T. Zhao e M.N. de Pinho, *Polymer* **40**, 6089-6097 (1999).
- [2] D.P. Queiroz, M.C. Gonçalves, and M.N. de Pinho, *J. Appl. Polym. Sci.* **103**, 315 (2007).
- [3] A.C. Trindade, M.H. Godinho, and J.L. Figueirinhas, *Polymer* **45**, 5551 (2004).
- [4] A.M. Figueiredo Neto, M.H. Godinho, T. Toth-Katona, and P. Palffy-Muhoray, *Braz. J. Phys.* **35**, 184 (2005).
- [5] C. Sena, C. Bayley, M.H. Godinho, J.L. Figueirinhas, P. Palffy-Muhoray, and A.M. Figueiredo Neto, *J. Magn. Magn. Mater.* **300**, 79-82 (2006).
- [6] C.Sena, M.H. Godinho, and A.M. Figueiredo Neto, *J. Appl. Phys.* **102**, 073524 (2007).
- [7] M.H. Godinho, J.L. Figueirinhas, C.T. Zhao, and M.N. de Pinho, *Macromolecules* **33**, 7675 (2000).
- [8] H. Finkelmann, H. Kock, and G. Rehage, *Makromol. Chem. Rapid. Commun.* **2**, 317 (1981).
- [9] F. Zhang and P.A. Heiney, *Phys. Rev. E* **73**, 021701 (2006).
- [10] A. Taborda, N. Louro, P.J. Sebastião, J.L. Figueirinhas, and M.H. Godinho, *Mol. Cryst. Liq. Cryst.* **450**, 119[319] (2006).
- [11] M.Zrínyi, L. Barsi and A. Büki, *J. Chem. Phys.*, 1996, **104**, 8750-8756.
- [12] V.T. Lebedev, Gy. Torok, L.Cser, A.L. Buyanov, L.G. Revelskaya, D.N. Orlova, A.I. Sibilev, *J. Magn. Magn. Mater.*, **1999**, *201*, 136-139.
- [13] M. Zrínyi, L. Barsi, A. Büki, *Polymer Gels and Networks*, 1997, **5**, 415-427.
- [14] S. Bohlius, H.R. Brand and H. Pleiner, *Phys. Rev. E*, 2004, **70**, 061411(1-10).
- [15] K.J. Suthar, M.K. Ghantasala, D.C. Mancini, and J. Ilavsky, *Proc. SPIE* **7289**, 72891D (1-9) (2009).
- [16] S. Ran, D. Fang, I. Sics, S. Toki, B.S. Hsiao, and B. Chu, *Rev. Sci. Instrum.* **74**, 3087 (2003).
- [17] A. Abragam, *The Principles of Nuclear Magnetism*, Clarendon Press Oxford, 1961
- [18] D. M. Sousa, G. D. Marques, J. M. Cascais, P. J. Sebastião, Submitted to *Rev. Sci. Instrum* (2009).
- [19] F. Noack, *Prog. Nucl. Magn. Reson. Spectrosc.*, **18**, 171(1986)
- [20] R. Kimmich and E. Ansaldo, *Prog. Nucl. Magn. Reson. Spectrosc.*, **44**, 257-320(2004)
- [21] B.D. Cullity, *Elements of X-Ray Diffraction*, second edition, Addison-Wesley Publ. Co. Inc. USA, (1978).

- [22] N. Fatkullin and R. Kimmich, *J. Chem. Phys.* **101**, 822 (1994).
- [23] M.H. Godinho, A.C. Trindade, J.L. Figueirinhas, L.V. Melo, P. Brogueira, A.M. Deus, and P.I.C. Teixeira, *Eur. Phys. J. E* **21**, 319-330 (2006).
- [24] D. Filip, P.J. Sebastião, C. Cruz, A.C. Ribeiro, M. Vilfan, T. Mayer, P.H.J. Kouwer, and G. Mehl, submitted to *Phys. Rev. E*.
- [25] F. Brochard and P.G. de Gennes, *J. Phys. (Paris)* **31**, 691 (1970).
- [26] A.M. Figueiredo Neto and M.M.F. Saba, *Phys. Rev. A* **34**, 3483 (1986).